RESEARCH ARTICLE

Editor's Choice

**ADVANCED
ENGINEERING
MATERIALS**

www.aem-journal.com

Investigation of the Structural Coating Homogeneity in Open-Porous Nickel/Polyurethane Hybrid Foams Produced by Flow-Controlled Electrodeposition

Francesco Kunz and Anne Jung*

In today's world, the saving of raw materials together with the reduction of emissions necessitates the development of new, customized and application-oriented materials which fulfill various requirements at the same time. Metal foams achieve a high strength combined with low weight. The present work deals with a flow-controlled production technique for hybrid foams to deposit a nanocrystalline nickel (Ni) layer on pre-treated, open-porous polyurethane (PU) foams. The analysis of the resulting coating thickness distributions with gravimetric and microscopic methods shows the qualitative and quantitative influences on the local deposition by varying the process parameters. For the first time, the coating thickness distribution of Ni/PU hybrid foams is investigated regarding the analysis of a global and local homogeneity. The comparison of experimental data with simulated flow velocity profiles leads to an estimation of the correlation between flow velocity, anode distance, and coating thickness distribution, which represents the mass transport. The correlations show, that the coating process is strongly controlled by the electrolyte's flow velocity as well as the distribution of the electric field.

1. Introduction

In the past few decades, the class of open-porous metal foams has continously gained more attention.[1,2] This type of material is nature-oriented and mimics the microstructure of trabecular bone or the skeleton of sea stars.[3] The stochastic distribution of pores within the foams leads to a very low density and a high surface-to-volume ratio.[2] The high inner surface allows the application as heat exchangers[4] and supports catalytic coatings in chemical engineering, as electrodes in lithium-ion batteries or fuel cells.[5] The high porosity and an outstanding stiffness to weight ratio of open-porous metal foams enable a particular application potential as lightweight construction material in the automotive, aerospace, and transportation industry.[3,6] In combination with their high energy absorption capacity, they can also be used as energy absorbers[3] for mechanical damping components and protective systems.[7] In future applications, lightweight metal foams could replace bulk materials which are used in crumple zones of cars as crash absorbers.[8] Therefore, the mechanical properties of open-porous metal foams are of particular interest. In the past, mostly aluminum (Al) foams were used as lightweight construction materials, but despite their good specific mechanical stiffness, the production is very expensive and complex. Furthermore, the production of Al foams does not always lead to a high reproducibility.[9]

To produce new hybrid materials, components with different properties are combined so that different specifications can be met at the same time. By using the Al foam with its natural, complex lightweight structure in combination with a thin coating of a nanocrystalline metal, the template structure is enormously reinforced regarding its mechanical properties and the reproducibility. The coating of foams can be accomplished by several methods like chemical and physical vapor deposition,[3,10] but especially the galvanic deposition provides a wide range of parameters to control and makes an industrial production possible.[11] The specific energy absorption capacity per foam thickness of developed hybrid foams increases through a 150 μm thick layer of nanocrystalline nickel (Ni) by a factor of 10 and per mass by a factor of more than 2 in comparison to uncoated 10 ppi Al foams.[11,12] The increased stiffness enhances compressibility, which is especially required for the application of hybrid foams in damping and energy absorption.

Uniaxial compression tests of single struts and pores show a reaction, which can be divided into three parts. The first part is a linear-elastic compression of the inner pores in a common plane with bending of the struts which are included in this pore layer. The force rises until the plastic collapses under stress, where damage occurs in the first layer of pores. At this point, the foam begins to deform plastically and undergoes constant stress with a continuous deformation of more pore layers. The stress at this time is defined as plateau stress, where the pores yield and

F. Kunz, A. Jung
Applied Mechanics - Foams and Metamaterials
Saarland University
Campus C 6.3, 66123 Saarbrücken, Germany
E-mail: anne.jung@mx.uni-saarland.de

The ORCID identification number(s) for the author(s) of this article can be found under https://doi.org/10.1002/adem.202200262.

**ADVANCED
SCIENCE NEWS**

www.advancedsciencenews.com

**ADVANCED
ENGINEERING
MATERIALS**

www.aem-journal.com

densificate layerwise until every pore layer is densificated.[11,13] The plateau stress phase characterizes the energy absorption on a nearly constant stress level and the applicability as a lightweight crash-absorbing material. Especially this part of the deformation behavior requires a constant coating thickness for a maximum dissipated energy and the usage as crash absorbers in the industry.[14] After the densification point, where all of the layers are compressed, the material behaves like a bulk material made of the same metal. The mechanical behavior of coated and uncoated Al foams was simulated with the help of the finite element method (FEM) by Jung et al.[9] Simulations of compression tests showed that most of the load during the tests is carried by the coating.[9] Since Al foams are very expensive in production and the struts have a marginal effect on the good properties of the hybrid foams, they are substituted by polyurethane (PU), which is a cheaper template material. Furthermore, the pre-treatment to enhance the surface conductivity and a general possibility to coat this surface is easier for PU foams than for Al foams.[9] A prior dip-coating process in graphite lacquer provides a conductive surface of the template material. The resulting pretreated PU foam is suitable for a further coating with nanocrystalline nickel through an electrodeposition process.[15] The galvanic coating procedure of the conductive PU foam in a static electrolyte causes an inhomogeneous coating thickness distribution and is only suitable for small specimens.[9,16]

Jung et al.[16] found that there occurs a higher coating thickness at the outer foam volume, which is a general problem during the electrodeposition of porous media. Depending on the position within a coated foam, the coating thickness of the foam center is only a tenth of the coating thickness in the outer area. This phenomenon was also observed by Karimi et al.[17] during the direct and pulsed current coating of open-porous PU foams with nickel. The inhomogeneity in coating thickness depends on the concentration of available nickel ions near the local cathode.[18] A limitation of the mass transport of ions into the inner part of the foam leads to a local depletion and a lower coating thickness. The local nickel ion concentration can be increased by the stronger dissolution of the anode material. In addition, a larger anode surface, which is arranged around the entire volume of the cathode, causes a higher mass transport. For the galvanic coating on Al foams, a cage-like sacrificial anode produces a more homogeneous distribution of the coating thickness in the resulting hybrid foams.[18] The development of the cage-like sacrificial anode for the deposition process on Al foams with a volume of $40 \times 40 \times 40 \, \text{mm}^3$ is also suitable for the coating process on PU foams. The production leads to an increasing coating thickness in the foam center up to 80%, but the volume of coatable foam is limited by the cage design and its geometry. The reason for the coating thickness distribution is explained by mass transport limitation, which occurs during the temporal evolution of the electrodeposition.[16,19,20] The transport of nickel ions, which is necessary to ensure a sufficient metal ion concentration for the deposition process is mainly driven by convection, diffusion, and migration.[21]

The differences in mass transport can also be described by the irregular propagation of the electric current on the porous electrode which causes a decreased movement of ions due to reduced migration effects. Euler[19,20] investigated the current distribution of a porous electrode and found a mostly symmetrical, reciprocal decrease to the inner of the cathode. Due to the inhomogeneous current distribution, the deposition rate of nickel ions decreases in the direction of the inner of the foam. This phenomenon is intensified by the electromagnetic shielding effects, because the electromagnetic permittivity decreases during the deposition of a metal layer of the foam geometry.

A possible solution to reduce the mass transport limitation produced by convection and diffusion is increasing the mass transfer coefficient with a flow of electrolyte through the open-porous foam during electrodeposition.[22–24] Thereby, fresh nickel ions can be delivered through the flow to increase the local concentration in the vicinity of the cathode surface. Zhu et al.[25] investigated a correlation of the internal flow velocity during a deposition with the mass transfer coefficient and found an exponential correlation.

The flow velocity of the electrolyte plays a major role during the electrodeposition process. Computational fluid dynamics (CFD) is a promising tool to calculate the flow velocity inside the reactor. The mass transport of nickel ions to the cathode surface due to convection can be estimated by qualitatively and quantitatively comparing the flow velocities of the electrolyte. Zhang et al.[26] previously studied the ion transport as well as the electrodeposition process in moving electrolytes and found that the mass transfer can reduce the diffusion layer near the electrode and increase the convection-dominated transport of ions and thus the efficiency of the electrodeposition process. For open-porous foams, the simulation is more complicated because the geometry is three-dimensional and complex. Sadeghi et al.[27] investigated the gas flow within open-porous foams. For the CFD simulation, they used micro-computed tomography (μ-CT) data similar to Della Torre et al.[28] to compute real geometries and found that CFD simulation provides reliable gas flow velocity patterns within the foams, but it is necessary to simulate a high number of pores, which produces a high computational effort. Especially for polymer electrolyte membrane fuel cells, the flow channels using open cellular foam materials are simulated with the help of CFD.[29] Wilberforce et al.[29] designed a fuel cell with the help of CFD software to optimize the flow uniformity and validated their results experimentally. Perez et al.[30] also investigated a flow cell with the help of CFD optimization to minimize the effect of electrolyte flow and current density edge effects and to simulate the concentration gradient within the flow cell. First experiments with a varied electrolyte flow through an open-porous, conductive-coated PU cathode with a diameter of 70 mm and a thickness of 20 mm have been conducted by Grill et al.[31] The local ion concentration was simulated and compared with experiments. The authors found, that the simulated distribution of ion concentration can be used to predict the coating ho.mogeneity, since a homogeneous ion concentration will lead to a more homogeneous coating of thickness distribution.

A general upscaling of the production process can only be achieved, if the mass transport limitation can be reduced. Therefore, the developed method of flow-controlled electrodeposition on open-porous cathodes is a very promising method, which can also be used for the structural optimization of complex 3D-printed geometries.[32–34]

This study summarizes the impact of different influencing factors on the electrodeposition of complex open-porous media and describes the optimization of the coating parameters for a homogeneous coating thickness distribution. The influence of

**ADVANCED
SCIENCE NEWS**

www.advancedsciencenews.com

**ADVANCED
ENGINEERING
MATERIALS**

www.aem-journal.com

a minimal flow inside the reactor as well as a moderate flow of 2.5 L min^{-1} and high flow velocity of 4.0 L min^{-1} was investigated. The moderate flow velocity corresponds to an electrolyte exchange time of approx. 6 min, the high flow velocity lowers the exchange time to ≈3.7 min. The two flow velocities are selected in the possible range of the delivery rate of the pump. They are adapted from Grill et al.[31] and were investigated in combination with a medium and a high anode distance. Furthermore, the influence of two different connection points for the current application to the cathode is compared using gravimetric and microscopic techniques.

2. Experimental Section

The main purpose of this contribution is the production of Ni/PU hybrid foams with flow-controlled electrodeposition as well as the subsequent structural characterization of the coating thickness distribution within the foam volume using gravimetric and microscopic analysis techniques. It is further necessary to compare the results of the produced specimens with corresponding CFD simulations of the flow velocity distribution inside the galvanic reactor to describe the effects of different flow velocity distributions and varying anode distances.

2.1. Specimen Preparation

PU foams (Schaumstoff Direkt Rüdiger Nolte, Enger, Germany) with a pore size of ≈10 ppi (pores per inch) were used as a precursor material for the coating process. The specimens were cut by a hot wire into a cylindrical, disc-like form with a diameter of 210 mm and a thickness of 40 mm. Prior to the electrodeposition process, a pre-treatment of the electrical unconductive polymer foam is necessary to produce a cathodic surface. For this purpose, the specimens were precoated with a layer of graphite conductive lacquer (Graphit 33, CRC Kontakt Chemie, Iffezheim, Germany) in a dip-coating process. To homogenize the thickness of the applied graphite layer after two dip-coatings and remove the superfluous varnish, the samples were dried 10 min under a constant air pressure with a moving airbrush from both sides of the disc-like foam. This drying device consists of a jet channel of 250 mm builded by a copper pipe and ≈100 cavities with a diameter of 1 mm drilled in a straight line, where the air flows out (see **Figure 1**a).

For the flow velocity-controlled electrodeposition, a self-constructed flow reactor with an edge length of 300 mm and a height of 338 mm was used. The inner free volume consisted of a hollow cylinder with a diameter of 237 mm. The inner volume of the reactor was 14.7 L. The reactor consisted of five modules machined out of polyoxymethylene (POM) with hollow cylinders of polymethyl methacrylate (PMMA) inside to guarantee a chemical inertness. The inlet and outlet were horizontally mounted at the bottom (inlet module 1) and the top (outlet module 5) of the reactor, so the electrolyte can be pumped through the volume externally. The two anode modules contained a titanium sheet bent along the inside of the hollow cylinder, which serves as contact and support for the anodes. The anodes were made of two sheets of titanium expanded metal and a layer of nonwoven fabric to ensure the filtration of anode sludge during the deposition. They were clamped onto a POM ring and filled with Ni
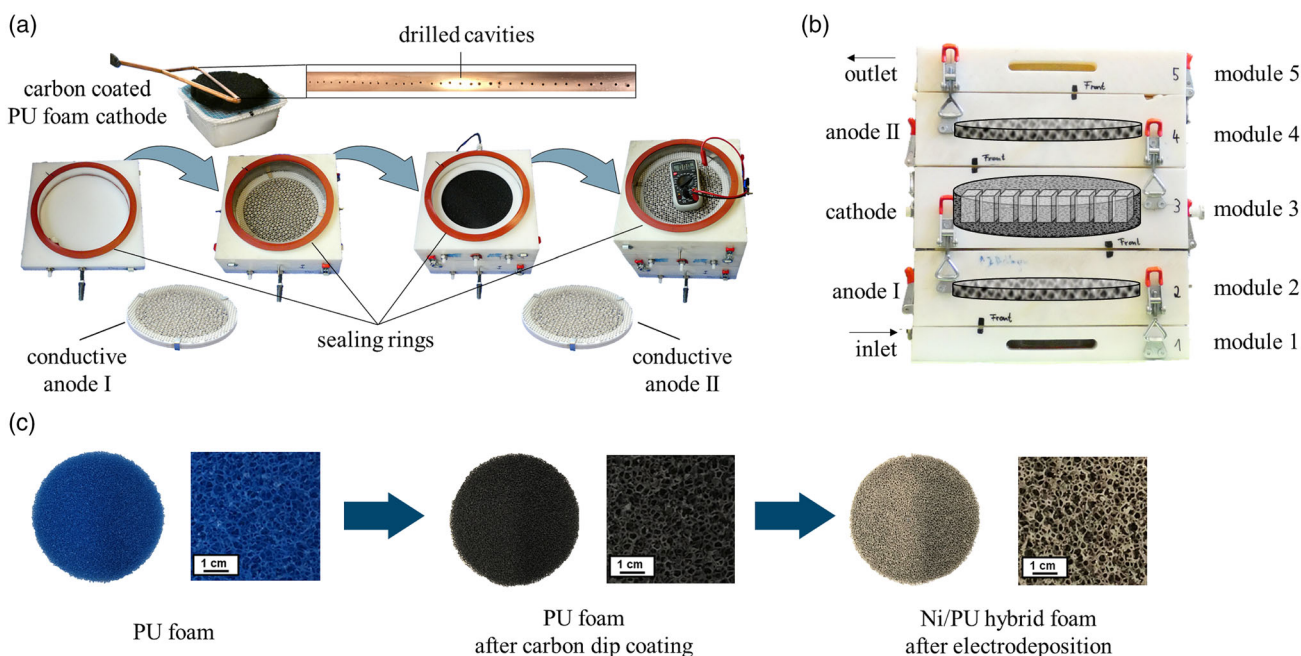

Figure 1. Workflow of electrodeposition on PU foams: a) The arrangement of both anodes and the carbon-coated foam cathode within the reactor modules, which are assembled with silicon sealing rings in between to ensure leak tightness. b) The flow reactor with its schematic arrangement of the anodes and the cathode. c) The foam cathode is placed between both anodes in the center of module 3 within the reactor. The evolution of the hybrid foam by coating with conductive carbon lacquer to ensure the conductivity during the production of the resulting Ni/PU hybrid foam.

pellets (A.M.P.E.R.E. GmbH, Dietzenbach, Germany). The cathode (module 3) was mounted with the clamped and wire-connected foam cathode in the middle of the reactor between both anodes. The workflow for the specimen preparation (a) as well as the reactor arrangement with all necessary modules (b) and the production route of the Ni/PU hybrid foam (c) is shown in Figure 1.

For the electrodeposition, a commercial nickel sulfamate electrolyte (Enthone GmbH, Langenfeld, Germany) with a nickel concentration of $110 \, g \, L^{-1}$ was used at a temperature of $50 \, °C$ and a pH of 3.8. The electrolyte was heated and stirred in an exchange vessel, which acted as an extern, temperated reservoir with stirring equipment. During the whole deposition process, the electrolyte inside the foam cathode was kept fresh by constant convection through the inlet and outlet of the reactor generated by a membrane pumping unit. Filtration through a cartridge filter with a nominal pore size of $10 \, \mu m$ ensured the elimination of small particles of anode sludge and other impurities, so the ion concentration in the vicinity of the cathode can be kept to a maximum level. The dried foam cathode was placed inside the cathode module and was electrically connected with four cables of the cathode at defined places in the volume. For the assembly of the whole reactor, the anode modules were filled with nickel pellets and were both connected to the anodic pole of the direct current power supply. The deposition was carried out at a current density of $1.65 \, mA \, cm^{-2}$ for $108.5 \, h$. The low current density was used to achieve the maximum in coating homogeneity for open-porous foams with a very complex inner structure. Jung et al.[9,35] found an enormous increase in the coating homogeneity from 44% to 61.3% in the foam center by decreasing the current density from 20 to $1 \, mA \, cm^{-2}$. Furthermore, the electrodeposition in nickel sulfamate baths at lower current densities showed lower inner stresses.[9] To determine the coating thickness gradient clearly, the foams were coated with an $\approx 220 \, \mu m$ thick nanocrystalline nickel layer, which is comparable high to standard coating thicknesses, but is necessary for an analysis of the occuring overcoating effects. After the coating procedure, the specimens were rinsed with water and dried by compressed air and an oven (Venti Line, VWR International LLC, Radnor, USA) at $50 \, °C$ for about $1.5 \, h$. The influence of flow velocity $\dot{v}$, anode distance d_{anodes}, coating thickness, and current connection on the homogeneity of the coating thickness in the hybrid foams was studied. Therefore, in the analysis of the structural characterization, it was differentiated between global, semi-local and local coating thickness distribution.

2.2. Coating Parameter Variation

The impact of different coating parameters was investigated by the characterization of the resulting coating distributions of all specimens of each foam plate. Further investigations have shown that the flow velocity has a strong influence on the coating homogeneity. The anode distance between both anodes and the cathode was studied. The current density was held constant due to the experimental factorial testing plan by Grill et al.[31] Since electrodeposition is a temporally determined process, two states of different coating thicknesses were investigated to allow conclusions of the kinetics of the coating on the homogeneity.

2.3. Structural Characterization of the Hybrid Foams

2.3.1. Global Coating Thickness Distribution

The produced, cylindrical Ni/PU hybrid foams were cut into cuboid specimens with a dimension of $20 \, mm \times 20 \, mm \times 40 \, mm$ by a bandsaw to analyze the gravimetric distribution of the coating layer depending on their position in the foam plate. For each cuboid specimen of the foam plate, the mass was measured with a balance as well as the determination of its dimensions by a caliper gauge. With this information, it is possible to calculate the specific density. The mass of the metallic coating dominates the mass of the polymer template, which is nearly constant for each specimen. The comparison of a defined number of specimens, which have been taken out of the same volume of every hybrid foam plate makes it necessary to calculate the density factor df. Therefore, the density of each local cuboid specimen was divided by the mean value of all considered specimens. The resulting density factor gave the information of the local deposited mass compared to the global deposited mass in relation to the corresponding volume. The developed data was analyzed with the help of a contour plot, so it was possible to compare the density distribution of hybrid foams within one foam plate and between the foams coated with different parameters.

2.3.2. Local Coating Thickness Distribution

The local distribution of the produced coating thickness was analyzed by the averaged coating thickness distribution of defined areas in the cross-section of each cuboid specimen extracted from the hybrid foam plate. The surface of the cross-section was mechanically grinded with a particle size of $\approx 15.3 \pm 1 \, \mu m$ with a water-cooled, rotary grinding tool (Phoenix Beta, Buehler, Esslingen am Neckar, Germany). An optical light microscope (VHX-7000 Digital Microscope, Keyence, Neu-Isenburg, Germany) was used in combination with a standard objective lense (VH-Z20R 20-200 objective lense, Keyence, Neu-Isenburg, Germany) and a magnification of 50. The software provided by the producer allows a panoramic image acquisition of the complete cross-section surface of each specimen prepared out of the foam plate. A requirement for the comparison of different specimens is the analysis of comparable areas. Therefore, the image of a foam specimen (see Figure 5) with a surface of $20 \, mm \times 40 \, mm$ was cropped and divided into ten sub-images with a dimension of $20 \, mm \times 4 \, mm$, which have been investigated regarding the coating thickness of the struts inside the foam. The local coating thickness of the stochastically distributed struts was measured by the ImageJ-based open source program Fiji. The measured values have been categorized by their position. Ten coating thickness values have been measured within each surface area to get a value of its average coating thickness.

2.4. Simulation of the Flow Velocity Distribution

In this study, the flow velocity distribution was compared to the thickness distribution of deposited nickel in hybrid metal foams. For the estimation of the flow velocity during the electrodeposition inside the reactor, a CFD simulation was used. The CFD

ADVANCED
SCIENCE NEWS
www.advancedsciencenews.com

ADVANCED
ENGINEERING
MATERIALS
www.aem-journal.com

Table 1. Boundary conditions in the simulation.

Type	Boundary	Value	Unit
Anode	Free Surface	0.13	–
Cathode	Permeability	1.45×10^{-8}	m^2
Electrolyte	Viscosity	2.1	Pa s
Flow	Volume Flow	2.5 & 4.0	L min^{-1}
Physics	Gravity	9.81	N kg^{-1}

software, developed by Autodesk, enables a computation of internal flow based on the geometry given in an .stl file. Boundary conditions were set analogue to the experiment. The simulation was conducted with incompressible flow, gravity, and defined flow velocities at the in- and outlet (see **Table 1**). The parameter for the porosity of the cathode and the anode were defined by using experimental data of free surface and Darcy's permeability measurements to obtain the whole flow distribution in the reactor, which can be used to compare the local flow velocity with local coating thickness. The solution was achieved with the help of the modified Petrov–Galerkin method. The flow velocity distribution was qualitatively compared in the cross-plane of the reactor and quantified by several measuring lines in the deposition plane.

3. Results and Discussion

3.1. Global Coating Thickness Distribution: Gravimetry

The gravimetric results show the distribution of the density factor in every foam plate, which represents the deposited amount of nickel averaged over the thickness of the investigated area. The contour plots in **Figure 2** show the global changes in density distribution caused by the variation of a flow velocity as well as the distance between both anodes and the cathode. A wide area of the foam plates is coated homogeneously between 90% and 110%, which means that the specific density of each local specimen slightly differs from the average specific density of all cuboid specimens in each investigated foam plate.

The density factor represents the amount of nickel that is deposited, since the PU template density varies negligibly over the entire volume and can be considered as constant. The resulting global distribution of the coating allows conclusions to be drawn about undercoated and overcoated areas in plane of the hybrid foam.

The overcoating at the edges of the foam plate increases with a higher flow velocity of the electrolyte (see Figure 2a,b). The edge overcoating effect is the highest at medium anode distances. The undercoated regions are located near the inlet of the reactor. In contrast, the overcoated areas are on the opposite side with a maximum distance to the inlet. Larger flow velocities also tend to be localized there. Furthermore, the variations in density increase with a higher flow velocity. The edge at largest distance to the inlet shows increased density factors in both experiments with a low anode distance. Hence, an increased flow velocity in combination with a medium anode distance causes a wider range of the specific density.

The range of the density factors within each foam plate (see **Table 2**) increases from 34.5% to 39.3%. The fraction of specimens f_{90}^{110} with nearly homogeneous density factor between 90% and 110% decreases from 68.4% to 59.6%, which implies that the variation of coating within the foam plate is larger at high
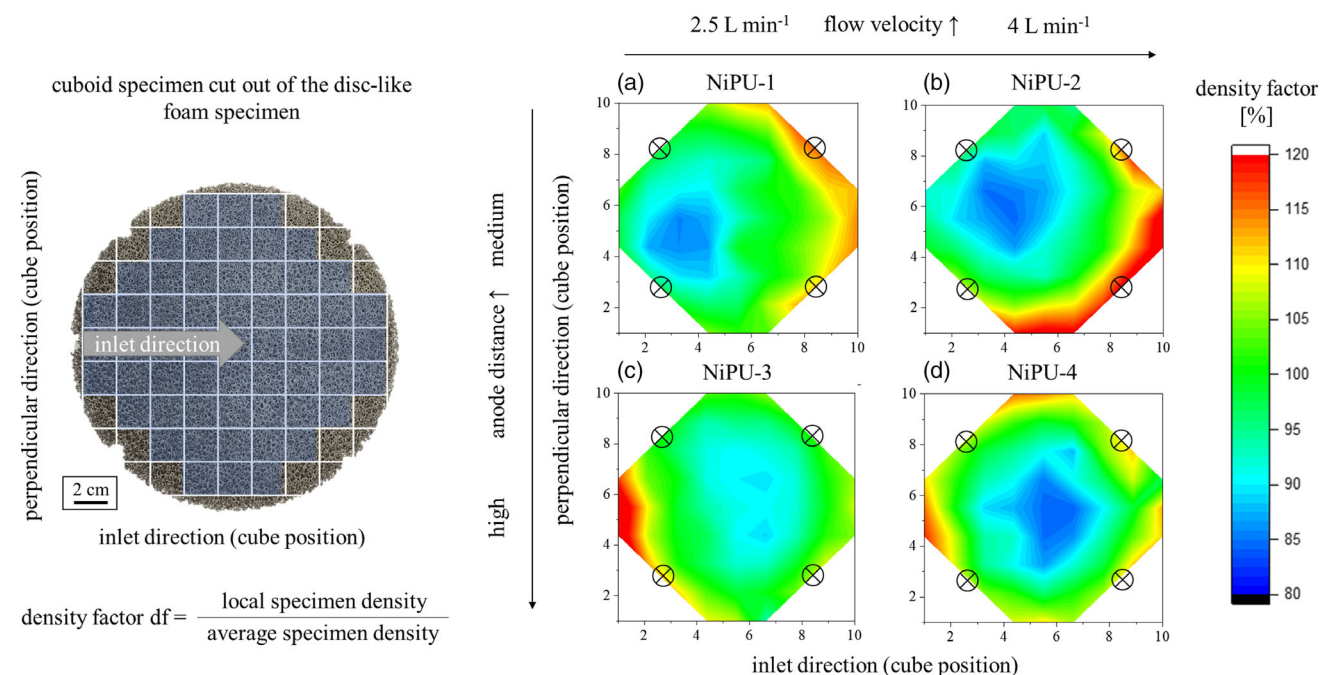

Figure 2. Disc-like hybrid foam specimen with cutting scheme for the cuboid specimens and the formula for the calculation of the density factor df (left). Gravimetric contour plots of the determined density distribution of four Ni/PU hybrid foams with different parameter sets (right). The black circles with a cross inside (⊗) mark the connection to the power supply.

ADVANCED
SCIENCE NEWS
www.advancedsciencenews.com

ADVANCED
ENGINEERING
MATERIALS
www.aem-journal.com

Table 2. Overview of the experimental parameters: electrolyte flow $\dot{v}$, anode distance d_{anodes}, connection points $\otimes$ to the power supply, minimum df_{min} and maximum df_{max} of the density factors determined in specimens produced with different coating parameters as well as the range of occurring density factors along with the fraction f_{90}^{110} of homogeneously coated cuboid specimens between 90% and 110%.

Specimen	$\dot{v}$	d_{anodes}	connection points	df_{min} [%]	df_{max} [%]	range [%]	f_{90}^{110} [%]
NiPU10-1	low	low	4 × out	85.6	120.1	34.5	68.4
NiPU10-2	high	low	4 × out	84.8	124.1	39.3	59.6
NiPU10-3	low	high	4 × out	89.0	127.1	38.1	87.7
NiPU10-4	high	high	4 × out	84.2	118.1	33.9	64.9
NiPU10-5	no	high	4 × out	79.5	120.1	40.6	70.2
NiPU10-6	high	high	1 × center	90.0	117.4	27.4	91.2

flow velocities. A high correlation of overcoating with the connection points to the power supply (marked as $\otimes$ in Figure 2) is also observable. This effect is superimposed in all four experimental results. Increasing the anode distance leads to a centralization of the areas with lower specific density to the middle of the foam plate shown in Figure 2c,d. Even if the inhomogeneity cannot be eliminated by an increased anode distance, the higher density factor and the associated overcoating at the edges can be reduced. The highest fraction of homogeneously coated foam specimens can be achieved with a low flow velocity and a high anode distance with 87.7%. An increasing flow velocity at high anode distances can decrease the range of density factor variation from 38.1% to 33.9%. Basically, a distribution with a lower coated center of the foam and slightly overcoated edges is given in every deposition. This leads to the assumption that the coating distribution is also highly influenced by the application of the electric current.

In addition to the influence of an increased flow velocity, the density distribution of the coating at minimum flow is investigated to identify a possible superimposed effect induced by the current distribution. For this purpose, a hybrid foam produced at a minimum flow rate of the electrolyte, which is at least necessary to keep the temperature constant inside the reactor, was produced and characterized regarding the gravimetrical

distribution. Furthermore, the effect of current application was investigated to turn out the effect of the current connection.

The gravimetrical analysis in **Figure 3**a shows an inhomogeneous density distribution over the foam plate. The density factor decreases from 120.1% at the outer edge near the current connection to 79.5% in the center of the foam plate which represents a range of 40.6%. The range of density factor df between the minimum density factor df_{min} and the maximum density factor df_{max} increases because of the lower coated center. Only 64.9% of the specimens have a density factor between 90% and 110%. The inhomogeneities occurring between the outer area of the foam plate and the center cannot be generated by differences in the flow velocity distribution, so they must arise by an inhomogeneous distribution of the electric field and edge effects, which often occur during electrodeposition processes. It is noticeable in all four density distributions of Figure 2 that the highest density factors are always located at the outer region of the plates, which represents the edges of the disc-like foam plate where the current is applied during the electrodeposition.[36–38] To reduce this effect, the cathodic connection to the power supply can be accomplished via the center of the foam as seen in Figure 3c. Thus, the distribution of the density factor is homogenized until minor deviations by a centralized current application. With a minimum specific density of 90% and a maximum specific density of 117.4%, the range of densities is the lowest with 27.4%. The fraction of homogeneously coated specimens can be enhanced up to 91.2% regarding the global homogeneity.

The frequencies of achieved density factors in the cuboid specimens within the investigated foam plates are shown in **Figure 4**. Diagram (a) represents the contour plots shown in Figure 2 of quantified information about the distribution of the density factors. Therefore, classes with a width of 5% are generated and the number of corresponding cuboid specimens with an adequate density factor is summarized. The ranges are represented by the width of the distribution, the height of the Gaussian fitting stands for the maximum number of samples with the corresponding density factor. Hence, a narrow distribution around 100% is optimal.

The highest number of homogeneously coated specimens can be achieved with a high anode distance and a low flow velocity
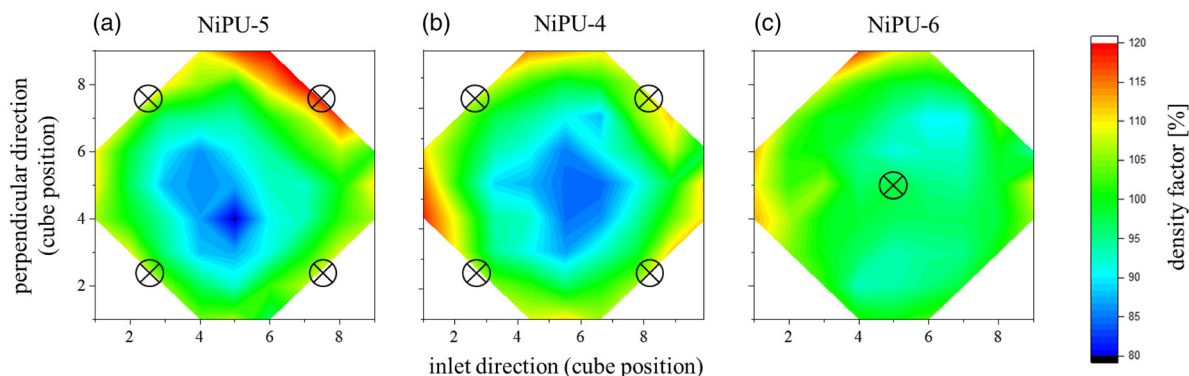

Figure 3. Gravimetric contour plots of the determined density distribution of Ni/PU hybrid foams produced with: a) minimal flow and b) 4.0 L min⁻¹ in combination with a current application at the edges. c) Optimized parameters of: b) with a central current application. The black circles with a cross ($\otimes$) inside mark the connection to the power supply.

**ADVANCED
SCIENCE NEWS**

www.advancedsciencenews.com

**ADVANCED
ENGINEERING
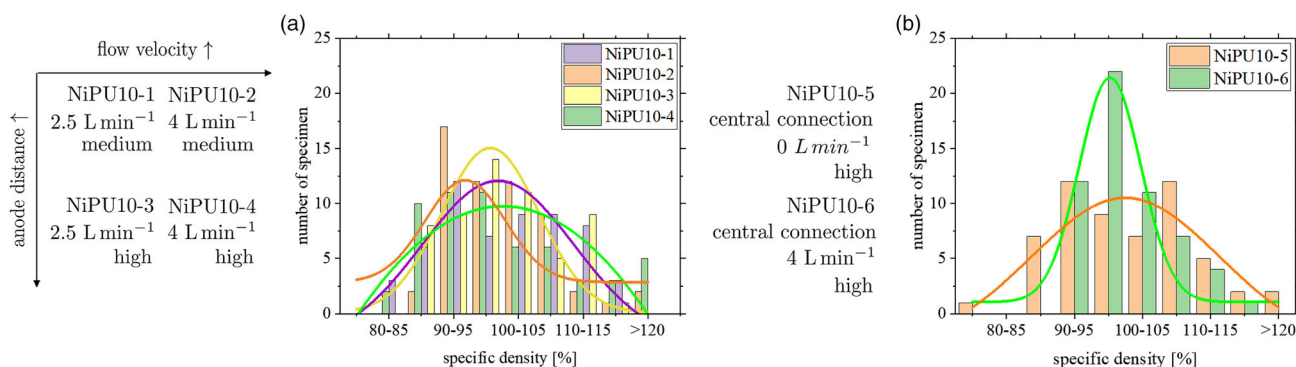MATERIALS**

www.aem-journal.com

Figure 4. Frequency plot of specific density factors determined in the previous experiments with varying process parameters: a) different flow velocities as well as a minimum flow velocity and b) current application with their corresponding Gaussian fits.

(NiPU10-3), if the specimens are connected to the power supply at four points at their edges. An increased flow of the electrolyte has no positive effect on the global density distribution. Only the central application of the current increases the homogeneity significantly until a number of 22 out of 57 specimens with a density factor between 95% and 100%.

The results of the gravimetry can be assessed as follows: The global gravimetry allows for a statement about the distribution of the coating within the entire volume of the coated foam plate. The distribution here has a 2D character regarding the foam plate surface and represents an averaged coating thickness distribution of the different cuboid specimens, which have been cut out of the whole foam plate. The global characterization of the density distribution shows that a high anode distance and a low flow velocity together with a central current source connection lead to the highest global homogeneity regarding the distribution of mass in the plane of the produced hybrid foam. To investigate the local distribution of the coating and thus also the density with regard to the thickness of the foam, a more detailed analysis of the 3D homogeneity is necessary to examine the gravimetrically characterized samples also spatially resolved microscopically.

3.2. Local Coating Thickness Distribution: Microscopy

A more detailed investigation of the coating thickness with respect to the thickness of the foam is shown in **Figure 5** and provides a local determination of the coating distribution. The diagrams represent three investigated cuboid specimens of different positions. The origin of each group of the specimen is described in Figure 5 (top). The specimens which are shown in Figure 5a are located near the electrolyte inlet of the flow reactor in a vertical distance of 2 cm away from the foam edge in the vicinity of the inlet. Figure 5b shows the specimen originated from the center of the foam plate at 10 cm and Figure 5c shows the distribution of the specimen which is located at the highest distance to the inlet at 18 cm.

Based on the thickness of the hybrid foam specimens, ≈75% are homogeneously coated with nickel. The central area of the foams is hardly influenced by the different coating conditions. In contrast, the outer 5 mm on both sides (bottom: 0–5 mm

and top: 35–40 mm) show highly overcoated areas. Especially the coating thickness at the bottom of the specimens (0–5 mm) deviates from the remaining parts. In contrast to the center of the foams, the coating thickness in this area depends strongly on the coating parameters. A significant reduction of the local overcoatings at the bottom of the foam specimens in all three positions in the foam plate can be achieved by increasing the flow velocity. The anode distance does also influence the local overcoating in a good way, but the effect strongly depends on the location in the foam plate. In the vicinity of the inlet, the effect of an increased anode distance is only dominant at low flow velocities. Increasing the flow velocity causes no big difference between both anode distances. In the center of the foam plate (see Figure 5b), the influence of the anode distance is higher with an increased flow velocity. In general, the overcoating at this position can be minimized by a high flow velocity and a high anode distance. Figure 5c shows the same trend for the overcoating tendencies at a high flow velocity. At a low flow velocity, the local coating thickness can be reduced by decreasing the anode distance.

The top area of the specimens is only affected by the increased flow velocity at the highest distance from the inlet. In this area, the flow velocity tends to be the highest, because the incoming electrolyte flows clashes against the reactor wall and moves in the direction of the foam and the outlet of the flow reactor. The deposition at the top area of the specimens extracted out of the center is not highly affected by changing deposition parameters. But in general, a higher flow velocity leads to a slightly thicker coating in this area. The transport of ions into the foam volume is mass-controlled. By increasing the flow velocity of the electrolyte, no significant increase in mass transport into the foam interior is observed. It can, therefore, be concluded that the decrease in coating thickness in the direction of the foam interior is due to further effects like the distribution of the electrical field in the foam volume and the Faraday shielding.

3.3. Semi-Global Coating Thickness Distribution: Microscopy

The global view of the density factor provides information about the distribution of the coating within the plane of deposition. The distribution of the coating within the thickness of the hybrid foam plate is summarized in one value. The more precise
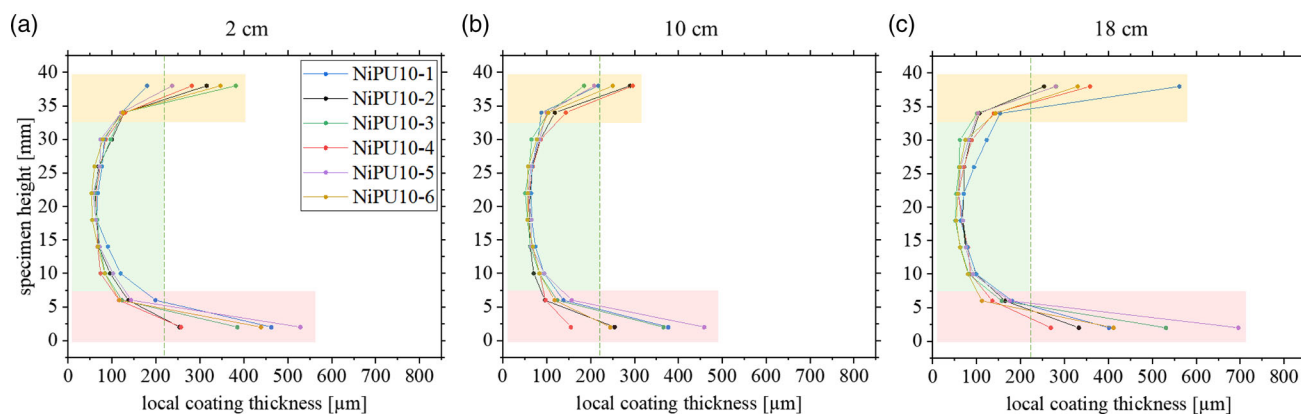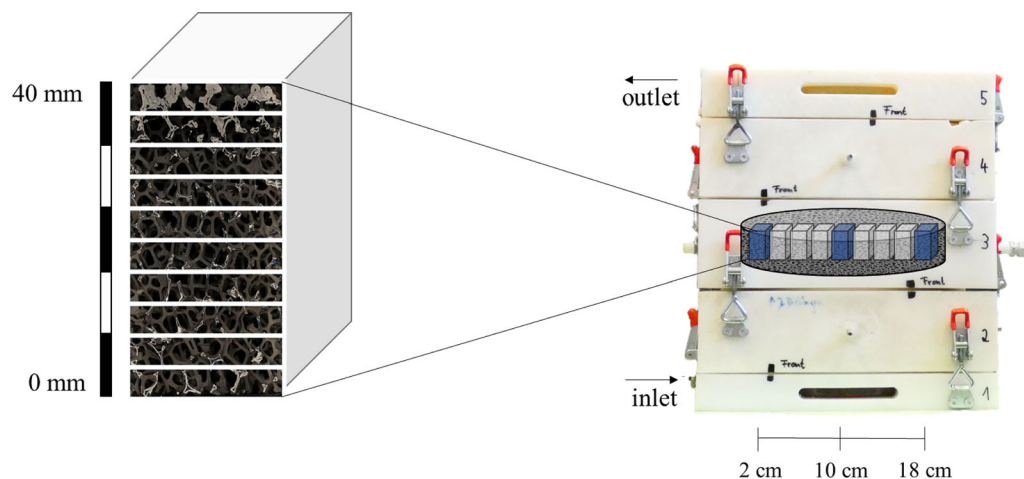
**ADVANCED
SCIENCE NEWS**

www.advancedsciencenews.com

**ADVANCED
ENGINEERING
MATERIALS**

www.aem-journal.com

Figure 5. Local coating thickness distribution of specimens at different distances away from the electrolyte inlet regarding their specimen height. The green dashed line shows the average theoretical coating thickness of 220 μm, the red marked areas represent the larger coated bottom of the specimens, the green area corresponds to the central areas, which are coated homogeneously and the yellow areas display the overcoated top of the cuboid specimens.

distribution of the coating thickness over the entire thickness of the foam necessitates a local as well as a semi-local analysis. While the local analysis characterizes the coating thicknesses in classes of a width of 4 mm, the semi-local analysis considers the tendency of the coating thickness in the outer as well as in the inner samples. For this purpose, the entire volume is investigated microscopically. As seen in **Figure 6**, three cuboid hybrid foam specimens have been extracted out of the middle area of the foam volume. The different positions of the extraction were defined by the distance to the inlet in the horizontal direction. One sample was extracted from each of the two edges and one from the planar center of the foam plate.

Each sample was analyzed microscopically over its entire cross-section. The resulting averaged coating thicknesses within the red marked area are shown in Figure 6.

An overview of the semi-local coating thickness distribution is given in **Table 3**. In addition to the averaged coating thickness values $\bar{d}_{top}$, $\bar{d}_{center}$, and $\bar{d}_{bottom}$ corresponding to the entire investigated area, the range of coating thicknesses is also shown. The range provides information on the homogeneity of the coating. The range is defined by the spread between the maximal and highest achieved coating thickness investigated in the corresponding area

of the three cuboid foam specimens at different distances from the inlet. The analysis of the top of the specimens shows that a low flow velocity in combination with a low anode distance leads to a wide range of the coating thickness. The achieved average coating thickness is 220.2 μm within a range of 207.1 μm. This range can be minimized by the maximization of the anode distances above and below the foam plane until an averaged coating thickness of 195.8 μm and a range of 108.5 μm. The increased anode distance leads to an enormous reduction of the overcoating and a corresponding range of values at low flow velocities. An increased flow velocity at low anode distances leads to a lower averaged coating thickness at the top (201.9 μm). With a higher anode distance, the value increases up to 224.6 μm. A higher flow velocity does enormously minimize the range of the investigated coating thicknesses at low (41.3 μm) and high anode distances (43.2 μm). The lowest coating thickness at the specimens top can be achieved with nearly no flow of electrolyte, which underlines the effect of the mass transport through a higher electrolyte flow. A central connection to the power source does not have a big influence on the reduction of overcoating in the top of the specimen, but the bottom and top show a symmetric distribution of coating by analyzing the semi-local coating thickness distribution.
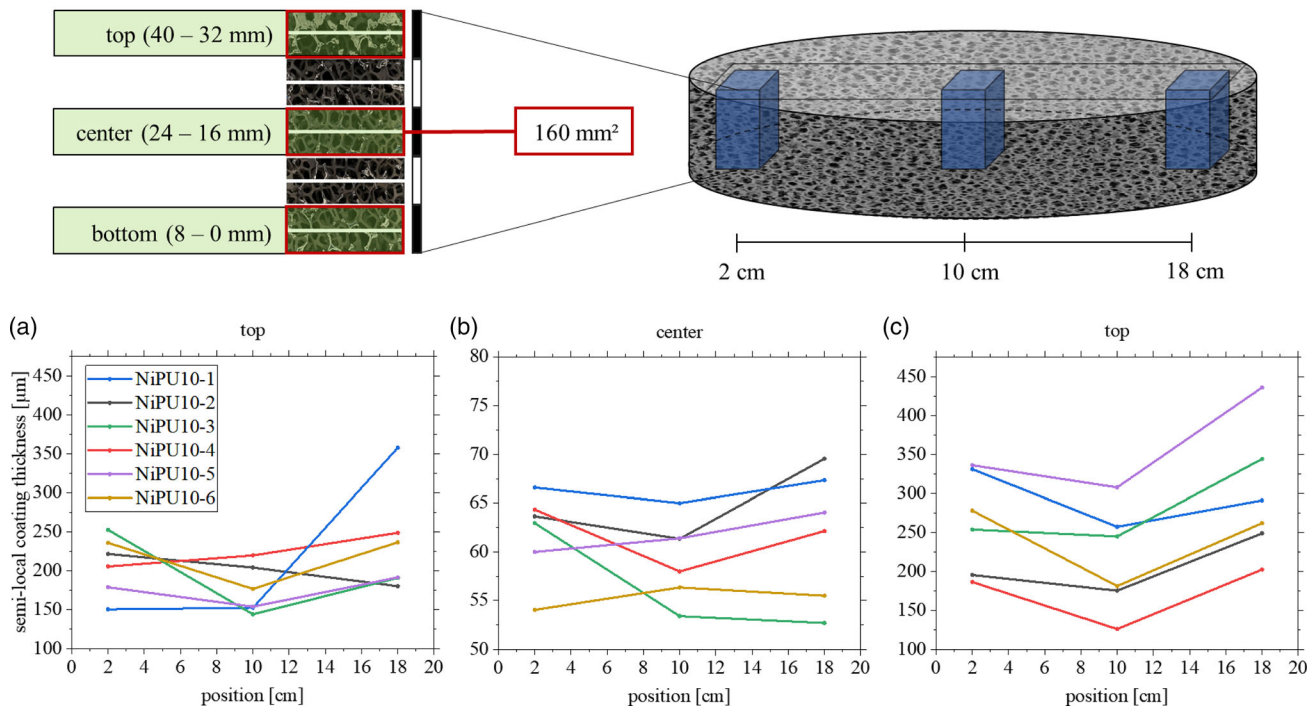
Figure 6. Top: Cuboid foam specimens were extracted from the hybrid foam plate at three defined positions at different distances from the electrolyte inlet (2 cm, 10 cm, 18 cm). The semi-global coating thickness was averaged over a cross-section surface of 160 mm² (red marked area) at the top, the center, and the bottom of each specimen. The analyzed area per each location (top, center, and bottom) consists of two cropped pictures with a dimension of 4 mm × 20mm for each picture. The resulting semi-local coating thickness was averaged over two pictures within the red marked area. Bottom: Semi-local coating thickness of the different coating conditions: Averaged coating thickness at the: a) top, b) center, and c) bottom of each specimen regarding different positions within the foam plane.

Table 3. Overview of the experimental parameter: electrolyte flow $\dot{v}$, anode distance d_{anodes}, connection points ⊗ to the power supply, and resulting coating thicknesses at the top $\overline{d}_{top}$, center $\overline{d}_{center}$, and bottom $\overline{d}_{bottom}$ of the specimens and the corresponding ranges within the investigated different distances to the inlet.

Specimen	$\dot{v}$	d_{anodes}	connection points	$\overline{d}_{top}$–range [µm]	$\overline{d}_{center}$–range [µm]	$\overline{d}_{bottom}$–range [µm]
NiPU10-1	low (↓)	low (↓)	4 × out (4c)	220.2–207.1	66.3–2.3	293.0–73.6
NiPU10-2	high (↑)	low (↓)	4 × out (4c)	201.9–41.3	64.9–8.2	206.5–73.7
NiPU10-3	low (↓)	high (↑)	4 × out (4c)	195.8–108.5	56.4–10.3	280.9–99.2
NiPU10-4	high (↑)	high (↑)	4 × out (4c)	224.6–43.2	61.5–6.4	171.6–76.4
NiPU10-5	no (↓↓)	high (↑)	4 × out (4c)	174.7–37.6	61.8–4.1	359.8–128.2
NiPU10-6	high (↑)	high (↑)	1 × center (cc)	216.3–59.9	55.3–2.3	240.3–96.8

The coating thickness in the center of the foam specimens varies between 55.3 µm with a central connection and 66.3 µm with low anode distance and low flow velocity. As a first conclusion, the deposition in the center of the specimens benefits from a low anode distance. Through the deposition process on the PU foams, shielding effects occur with a higher coating thickness, which leads to a reduced mass transport in the inner of the foam. A decreasing coating thickness can increase the inner coating thickness of the foam volume because of a reduced shielding, but a side effect of reducing the distance between anode and cathode is an inhomogeneous flow distribution. The reduced mass transport is manifested in a reduced coating thickness in the foam center. The bottom of the specimens is most affected by changing the parameters. In this study, the increased flow velocity has a high influence on the absolute coating thickness, which is reduced at both anode distances. At a low anode distance, the averaged thickness can be reduced from 293.0 to 206.5 µm. With a higher anode distance, the thickness can be reduced from 280.9 to 171.6 µm. The highest coating thickness of 359.8 µm prevails with a minimal flow, which implies that a general flow has a reductive effect on overcoating. With these parameters, also the range of thickness values is the highest with 128.2 µm, which represents a high inhomogeneity. The central connection of the foam produces moderate values 240.3 µm and a strongly reduced range of 96.8 µm.

**ADVANCED
SCIENCE NEWS**

www.advancedsciencenews.com

**ADVANCED
ENGINEERING
MATERIALS**

www.aem-journal.com

The increase of the anode distance at low flow velocities leads to a weakened electrical field and a lower overcoating tendency. At higher flow velocities, the flow of the electrolyte dominates over the anode distance leading to a higher coating thickness of the upper area of the foam specimens. An explanation for this phenomenon is mass transport, which is supported through the electrolyte flow. The bottom area of the foam, which faces the fresh electrolyte that flows in through the inlet, is coated less. Despite the higher concentration of nickel ions at the bottom, the layer growth is inhibited because the ad-atom adhesion is reduced by the increased local flow velocity. Especially at high flow velocities, there exists a positive effect of an increased anode distance.

3.4. Simulation of the Flow Velocity Distribution

As seen in the global and local as well as in the semi-local homogeneity characterization, there is a huge dependency on the coating distribution, which is affected by the distribution of the flow velocity inside the reactor. For the qualitative correlation of the mass distribution within the foam plane with the flow velocity, the velocity distribution is simulated with a CFD tool. **Figure 7** shows the simulated absolute flow velocities inside the reactor in its cross-section as well as the z-components of the flow velocities in the foam plane, where the deposition takes place.

The absolute velocity in Figure 7a shows that the highest value is located near the inlet at the bottom of the reactor, where the electrolyte is pumped into the reactor volume. The velocity decreases with the reactor height due to the arrangement of both anodes and the foam cathode, which each acts like a diffusor with a limited permeability. With the first anode, the flow velocity is reduced due to the free surface (see **Figure 8**) of the triple points between the nickel pellets, which are placed between the two titanium expanded metal pieces.

Also, the non-woven material around the anodes reduces the flow but also leads to a homogenization of the flow distribution with its limited permeability. An increase in the anode distance leads to an earlier homogenization process, so the flow velocity distribution of the electrolyte which reaches the plane of the cathode is more even. Higher flow velocities produced by more pumping lead to a generally higher flow into the reactor, but also through the cathode. The effect of flow homogenization through the anodes decreases at higher velocities, though the flow velocity distribution within the plane of the cathode is more inhomogeneous at high flow velocity, but the general flow velocity in the plane of the cathode, which is necessary to determine the effects of mass transport and drives the reduction of overcoating can be increased.

The flow velocity distribution in the plane of the foam (see Figure 7b) shows the absolute flow velocity distribution in the z-direction in the area of the electrodeposition process. There is a high gradient from one side to the other observable side, like in the distribution of the cross-section of the reactor. The z-component of the velocity vector dominates the deposition process, since the mass transport of the ions into the foam happens mainly in this direction. The right area of the plane (see Figure 7b) far from the inlet shows the highest flow velocity, because the electrolyte flows toward the opposite reactor wall and is deflected upwards. Although the permeability of the anode can impede the resulting velocity gradient, there is still a significant difference in the foam plane. For both large and medium distances between the anodes, the distribution shows a notable difference in flow velocity, which is also distinct in the gravimetric analysis in Figure 2. The z-velocity distribution in the foam plane in Figure 7b outlines an outer ring of low velocity at a medium distance between anode and cathode. An increased distance reduces the difference in the velocity between the inner and outer area, but there is a gradient in the foam plane remaining.
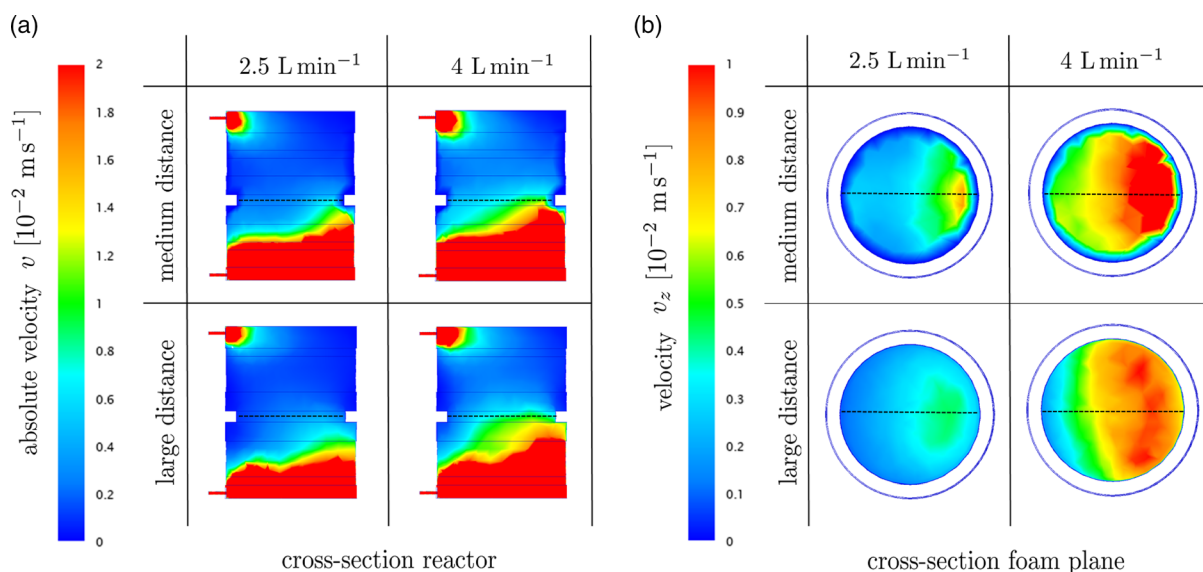

Figure 7. Simulation of the flow velocity distribution for varying flow velocities and anode distances: a) absolute flow velocity in the cross-section of the reactor (the investigated inlet plane is marked with a black dashed line) and b) z-velocity within the cross-section of the foam plane (the investigated inlet direction is marked with black dashed line).
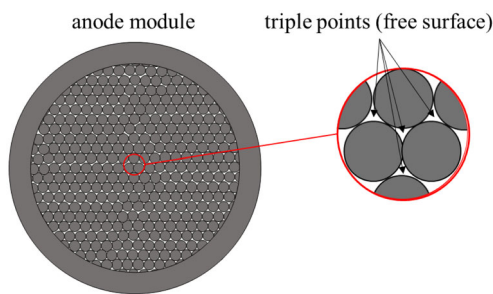
Figure 8. Schematically shown 2D distribution of nickel pellets within the anode: The electrolyte flows through the triple points between nickel pellets which are represented in 3D as spheres.

The flow velocity can also be analyzed numerically. **Figure 9**a shows the different absolute flow velocities in the middle of the deposition plane in the reactor for the four different parameter sets. Enlarging the distance between anode and cathode reduces the velocity gradient inside the foam plane. An increasing distance between the anodes and the foam cathode also changes the curvature in the velocity distribution from convex to concave. This means that the gradient in the foam plane is reduced, but even at a maximum anode distance at both flow velocities, there is a difference remaining. Figure 9b shows the different components in the x-, y-, and z-direction of the absolute velocity vector for the different parameter sets. In all four cases, the dominant component of the velocity vector is the z-component. Since the flow through the reactor is vertically upward, the velocity direction is dominated in this direction. Especially in the range of the maximum flow velocity, deviations of the x- and y- velocities occur, which indicates local turbulences. Since mass transport dominates in the z-direction, the effect on deposited volume

is locally negligible, but the turbulence in the flow can affect the nucleation rate as well as grain growth due to reduced adsorption of atoms during the nucleation process. The higher flow velocity in the positions far from the inlet in the right area correlates with the higher mass of coated volume, which is represented in the gravimetrical analysis. Furthermore, the maximum amount of global coating is represented at these positions within the different specimens. Especially these areas of higher flow velocity, which are represented near the bottom of the specimens, show a reduced overcoating at the edges. It implies that the reduction of the nucleation rate by a higher flow of electrolyte dominates over the mass transport. The flow velocity distribution is a promising approach to estimate the deposition rate. An increasing flow velocity through the inlet leads to a higher absolute velocity of the electrolyte in the foam plane of the electrode-position and partially improved homogeneity of the produced hybrid foams.

3.5. Optimized Parameters with Theoretical Optimum in Coating Thickness

Previous results have shown that the overcoating can be reduced by higher flow velocities. Higher flow velocities do also require an increased distance between both anodes and the cathode, since this allows homogenization of the flow velocity distribution of the electrolyte. The high flow velocity and the maximum anode spacing reduce overcoating and increase the probability of mass transport to the inner of the foam at the same time without causing a too strong flow nonuniformity. Furthermore, the contacting of the specimen with the power supply also plays a major role. The experiments on a central connection have shown a positive effect on the global homogeneity. The optimized parameter resulting from the experiments leads together with the reduction
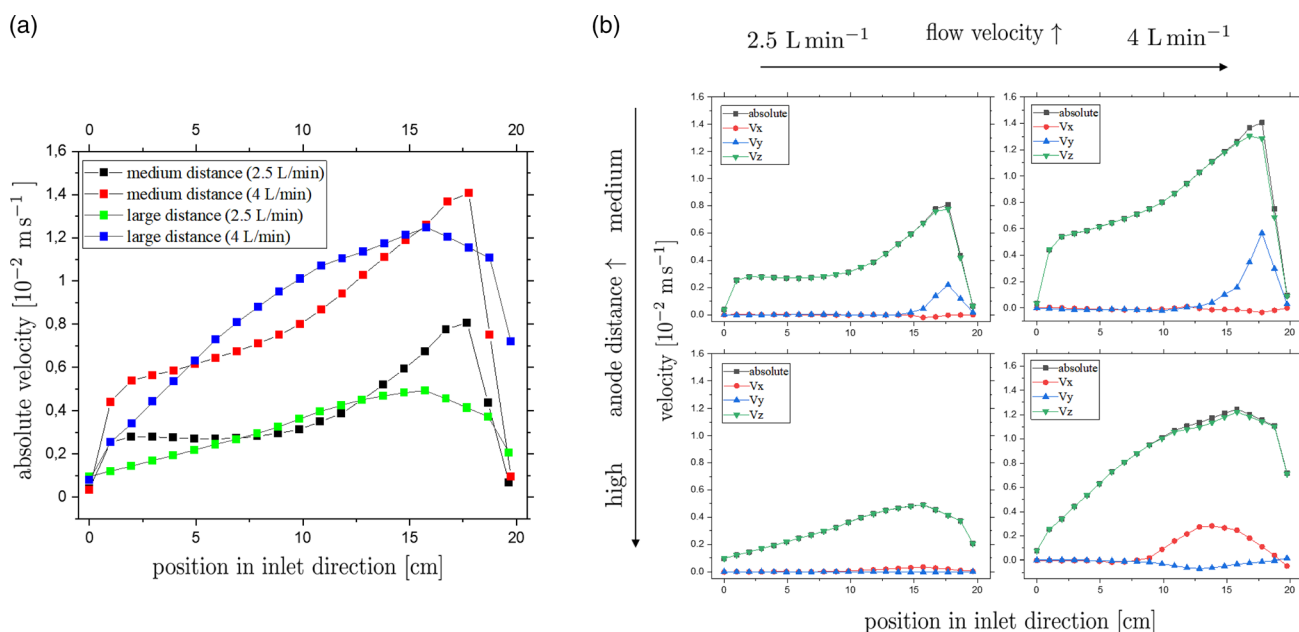

Figure 9. Flow velocity distributions inside the reactor: a) Simulated absolute velocities in the inlet plane for the four different parameter sets and b) x-, y-, and z-components of the velocity vector for the corresponding parameters.

ADVANCED
SCIENCE NEWS
www.advancedsciencenews.com

ADVANCED
ENGINEERING
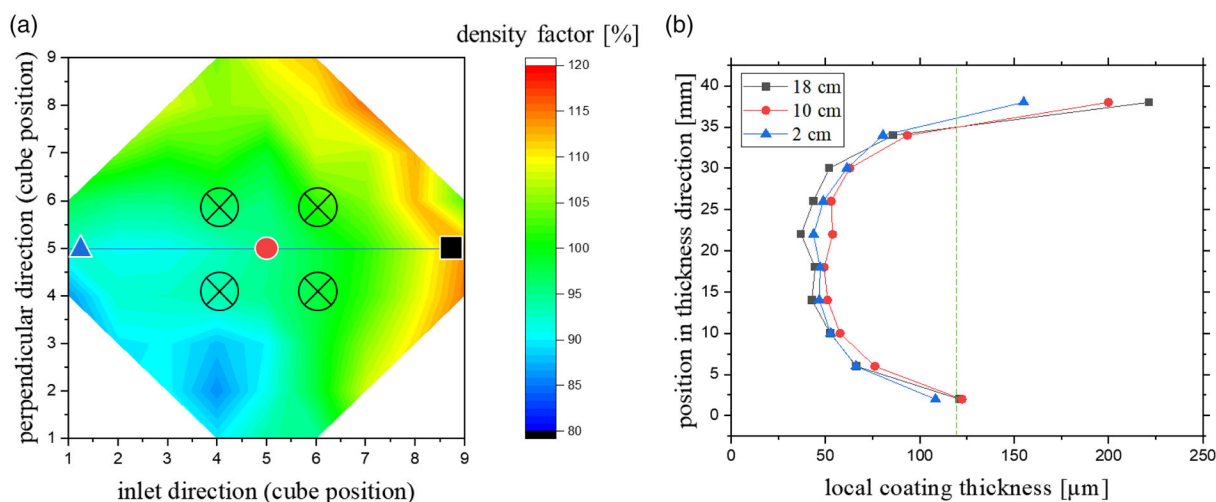MATERIALS
www.aem-journal.com

Figure 10. Optimized process parameters together with a moderate theoretic coating thickness of 120 μm show a more homogeneous distribution of the density factor within a foam plate and reduced overcoating over the thickness of the foam. The green dashed line shows the average theoretical coating thickness of 120 μm.

of theoretical coating thickness to a more uniformly coated hybrid foam.

Figure 10a represents the gravimetrical analysis, where the connection to the power supply is marked with crossed circles. Additionally, three specimens have been investigated regarding their microscopic coating thickness distribution over the foam thickness. The gravimetry shows a wide range of uniformly coated specimens with a density factor around 100% and a less significant undercoating in the middle of the specimen. Furthermore, the overcoating in the outer areas is reduced. The global inhomogeneity at the right edge of the specimen correlates to the area with the higher flow velocity. The area with a lower coating is analogous to this in the area of lower flow velocities. Figure 10b shows the correlating coating thickness distributions. According to the gravimetric distribution, the inhomogeneity which is represented in Figure 10a is also visible in the coating thickness at the top of the three cuboid specimens. Generally, the coating thickness a the top of the specimen is dominating the overcoating effect, because the coating thickness at the bottom is nearly the same in all specimens. The coating at the top is the highest at the position farthest from the inlet position. The center specimen shows a slightly reduced overcoating and the specimen in the vicinity of the inlet is minor overcoated.

4. Conclusion

Hybrid metal foams were produced in a galvanic flow-controlled reactor. The structural homogeneity was investigated on different scales. The results of gravimetric analyses depicting the global distribution of deposited nickel in the local volume show that the global inhomogeneities differ locally. In general, a distribution can be observed where edges have higher densities than inner regions. These effects are due to the distribution of the electric current on the specimen surface. In highly curved regions, such as exist at edges, the specific density increases due

to higher current densities.[36–40] Furthermore, the general homogeneity is also influenced by local differences in the electrolyte flow velocity. Areas with higher flow velocities have higher specific densities in the total volume. An increase in the anode distance generally leads to a homogenization of the global coating distribution. The highest percentage of globally homogeneous coated specimens was obtained by central contacting with the power supply. This indicates that the inhomogeneous distribution of the current on the cathode surface can be corrected via the current application.

The investigation of the local coating thickness clearly shows that the overcoating of the bottom side of the specimen can be reduced enormously by increasing the flow velocity. In this area, increasing the anode spacing leads to a further homogenization of the coating thickness distribution. The qualitative variation of the coating thickness inside the specimens is similar in all experiments. Only the reduction of the anode distance leads to a later decrease in the coating thickness.

The semi-local study of the coating thickness has shown that the largest changes can be detected at the bottom of the hybrid foam plates. The most promising parameters here are a high anode spacing and a high flow rate. The upper area of the plates is affected to a rather minor extent. In the center of the plates in relation to their thickness, the maximum coating thickness can be achieved by smaller anode distances, which indicates a positive effect of a high density of the electric field.

The CFD simulations show clear areas of higher velocities when analyzing the flow within the reactor. The distribution is similar to the gravimetric results, which suggests a correlation between mass transport and convection caused by the flow of electrolytes. On the one hand, the increase of the anode spacing leads to a homogenization of the distribution of the flow velocity within the deposition plane, but a general difference remains. If the parameters, which were identified as optimized with a high theoretical coating thickness are transferred to experiments with

lower coating thickness, the global and local homogeneity can be further improved. In addition, the gravimetric data correlate well with the microscopic measurements. Only the general decrease of the coating thickness toward the interior of the specimen remains due to shielding effects. The characterization of shielding effects needs future research.

Conflict of Interest

The authors declare no conflict of interest.

Data Availability Statement

The data that support the findings of this study are available from the corresponding author upon reasonable request.

[1] J. Banhart, G. S. Vinod-Kumar, P. H. Kamm, T. R. Neu, F. García-Moreno, *Cienc. e Tecnol. dos Mater.* **2016**, *28*, 1.

[2] L. P. Lefebvre, J. Banhart, D. C. Dunand, *Adv. Eng. Mater.* **2008**, *10*, 775.

[3] M. F. Ashby, A. G. Evans, N. A. Fleck, L. J. Gibson, J. W. Hutchinson, H. N. G. Wadley, *Metal Foams : A Design Guide*, Butterworth-Heinemann, Oxford, **2000**.

[4] S. Rashidi, M. H. Kashefi, K. C. Kim, O. Samimi-Abianeh, *Appl. Energy* **2019**, *243*, 206.

[5] W. Yang, S. Yang, W. Sun, G. Sun, Q. Xin, *Electrochim. Acta* **2006**, *52*, 9.

[6] J. Banhart, *Prog. Mater. Sci.* **2001**, *46*, 559.

[7] M. Reinfried, G. Stephani, F. Luthardt, J. Adler, M. John, A. Krombholz, *Adv. Eng. Mater.* **2011**, *13*, 1031.

[8] J. Liu, Y. Li, X. Gao, P. Liu, L. Kong, *Int. J. Crashworthiness* **2015**, *20*, 325.

[9] A. Jung, S. Diebels, *Adv. Eng. Mater.* **2016**, *18*, 532.

[10] X. Liu, X. Du, X. Wang, N. Li, P. Xu, Y. Ding, *Biosens. Bioelectron.* **2013**, *41*, 848.

[11] A. Jung, H. Natter, S. Diebels, E. Lach, R. Hempelmann, *Adv. Eng. Mater.* **2011**, *13*, 23.

[12] B. A. Bouwhuis, J. L. McCrea, G. Palumbo, G. D. Hibbard, *Acta Mater.* **2009**, *57*, 4046.

[13] S. Heinze, T. Bleistein, A. Düster, S. Diebels, A. Jung, *ZAMM Z. Angew. Math. Mech.* **2018**, *98*, 682.

[14] A. Jung, S. Bronder, S. Diebels, M. Schmidt, S. Seelecke, *Mater. Des.* **2018**, *160*, 363.

[15] A. Jung, Z. Chen, J. Schmauch, C. Motz, S. Diebels, *Acta Mater.* **2016**, *102*, 38.

[16] A. Jung, M. Koblischka, E. Lach, S. Diebels, *Int. J. Mater. Sci.* **2012**, *2*, 97.

[17] E. Z. Karimi, F. Barzegar, A. Moloodi, R. Zolfaghari, *Metall. Mater. Trans. B Process Metall. Mater. Process. Sci.* **2021**, *52*, 3439.

[18] A. Jung, D. Klis, F. Goldschmidt, *J. Magn. Magn. Mater.* **2015**, *378*, 178.

[19] K. J. Euler, *Chemie Ing. Tech.* **1965**, *37*, 626.

[20] K. J. Euler, *Electrochim. Acta* **1973**, *18*, 385.

[21] R. T. Choo, J. M. Toguri, A. M. El-Sherik, U. Erb, *J. Appl. Electrochem.* **1995**, *25*, 384.

[22] R. A. Marquez-Montes, K. Kawashima, Y. J. Son, J. A. Weeks, H. H. Sun, H. Celio, V. H. Ramos-Sánchez, C. B. Mullins, *J. Mater. Chem. A* **2021**, *9*, 7736.

[23] I. Khazi, U. Mescheder, J. Wilde, *Materials* **2021**, *14*, 14.

[24] B. S. Vishnugopi, F. Hao, A. Verma, P. P. Mukherjee, *Phys. Chem. Chem. Phys.* **2020**, *22*, 11286.

[25] P. Zhu, Y. Zhao, *Adv. Eng. Mater.* **2017**, *19*, 12.

[26] H. Zhang, N. Zhang, F. Fang, *Precis. Eng.* **2021**, *72*, 122.

[27] M. Sadeghi, M. Mirdrikvand, G. R. Pesch, W. Dreher, J. Thöming, *Exp. Fluids* **2020**, *61*, 1.

[28] A. Della Torre, G. Montenegro, G. R. Tabor, M. L. Wears, *Int. J. Heat Fluid Flow* **2014**, *50*, 72.

[29] T. Wilberforce, F. N. Khatib, O. S. Ijaodola, E. Ogungbemi, Z. El-Hassan, A. Durrant, J. Thompson, A. G. Olabi, *Sci. Total Environ.* **2019**, *678*, 728.

[30] T. Pérez, L. F. Arenas, D. Villalobos-Lara, N. Zhou, S. Wang, F. C. Walsh, J. L. Nava, C. P. de León, *J. Electroanal. Chem.* **2020**, *873*, 1.

[31] C. Grill, M. Fries, A. Jung, S. Diebels, *Int. J. Heat Mass Transf.* **2021**, *180*, 121791.

[32] S. Bronder, F. Herter, D. Bähre, A. Jung, *Adv. Eng. Mater.* **2022**, submitted.

[33] S. Bronder, M. Adorna, T. Fíla, P. Koudelka, J. Falta, O. Jiroušek, A. Jung, *Adv. Eng. Mater.* **2021**, *23*, 5.

[34] S. Grednev, S. Bronder, F. Kunz, M. Reis, F. Welsch, S.-M. Kirsch, S. Seelecke, S. Diebels, A. Jung, *GAMM* **2022**, submitted.

[35] A. Jung, H. Natter, R. Hempelmann, S. Diebels, R. Koblischka, U. Hartmann, E. Lach, *J. Phys. Conf. Ser.* **2010**, *200*, 8.

[36] K. M. Yin, J. H. Wei, J. R. Fu, B. N. Popov, S. N. Popova, R. E. White, *J. Appl. Electrochem.* **1995**, *25*, 543.

[37] Y. J. Tan, K. Y. Lim, *Surf. Coatings Technol.* **2003**, *167*, 255.

[38] M. S. Rajput, P. M. Pandey, S. Jha, *Int. J. Adv. Manuf. Technol.* **2015**, *76*, 61.

[39] Y. Cheng, X. Luo, J. Betz, S. Buckhout-White, O. Bekdash, G. F. Payne, W. E. Bentley, G. W. Rubloff, *Soft Matter* **2010**, *6*, 3177.

[40] J. O. Dukovic, *IBM J. Res. Dev.* **1990**, *34*, 693.